Article:
Rymaruk, M.J., O'Brien, C.T., Brown, S.L. et al. (2020) RAFT dispersion polymerization of benzyl methacrylate in silicone oil using a silicone-based methacrylic stabilizer provides convenient access to spheres, worms, and vesicles. Macromolecules, 53 (5). pp. 1785-1794. ISSN: 0024-9297

https://doi.org/10.1021/acs.macromol.9b02697

RAFT dispersion polymerization of benzyl methacrylate in silicone oil using a silicone-based methacrylic stabilizer provides convenient access to spheres, worms and vesicles

Matthew J. Rymaruk,*[a] Cate T. O'Brien, [a] Steven L. Brown,[b] Clive N. Williams[b] and Steven P. Armes.*[a]

a. Dainton Building, Department of Chemistry, University of Sheffield, Brook Hill, Sheffield, South Yorkshire, S3 7HF, UK.

b. Scott Bader Company Ltd, Wollaston, Wellingborough, Northamptonshire, NN29 7RL, UK.

* Authors to whom correspondence should be addressed (s.p.armes@sheffield.ac.uk or m.rymaruk@sheffield.ac.uk)

For use as the table of contents graphic only

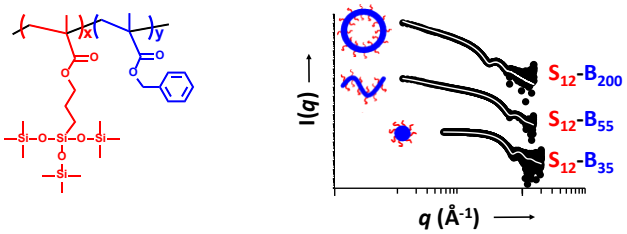

Abstract. Reversible addition-fragmentation chain transfer (RAFT) solution polymerization of 3-[tris(trimethylsilyloxy)silyl] propyl methacrylate (SiMA) was conducted in toluene in order to prepare three PSiMA precursors with mean degrees of polymerization (DP) of 12, 13 or 15. Each precursor was then chain-extended in turn via RAFT dispersion polymerization of benzyl methacrylate (BzMA) in a low-viscosity silicone oil (decamethylcyclopentasiloxane, D5). ^{1}H NMR studies confirmed that such polymerizations were relatively fast, with more than 99 % BzMA conversion being achieved within 100 min at 90°C. Moreover, GPC analysis indicated that these polymerizations were well-controlled, with dispersities remaining below 1.25 when targeting PBzMA DPs up to 200. A phase diagram was constructed at a constant copolymer concentration of 20% w/w. When the $PSiMA_{15}$ stabilizer was utilized, only spherical micelles were accessible as determined by transmission electron microscopy (TEM) and small-angle X-ray scattering (SAXS) studies. Nevertheless, these spheres exhibited narrow size distributions and tunable intensity-average diameters ranging between 19 and 49 nm, as determined by dynamic light scattering (DLS). In contrast, spheres, worms or vesicles could be prepared depending on the target PBzMA DP when utilizing the relatively short $PSiMA_{12}$ precursor. Moreover, each of these nano-objects could be obtained at copolymer concentrations as low as 5% w/w. To obtain more detailed structural information, these spheres, worms and vesicles were further characterized by small-angle X-ray scattering (SAXS). $PSiMA_{12}$-$PBzMA_{55}$ worms formed reasonably transparent free-standing gels when prepared at copolymer concentrations as low as 5% w/w and exhibited an elastic modulus (G') of 90 Pa at 25°C as judged by oscillatory rheology studies. Finally, broadening of the molecular weight distribution was observed during the long-term storage of PSiMA-PBzMA dispersions at ambient temperature. We tentatively suggest that this instability is related to hydroxyl impurities in the SiMA, which leads to crosslinking side-reactions. This problem also causes incipient flocculation of the spheres and worms during long-term storage of such dispersions.

Introduction

It is well-known that AB diblock copolymer chains can self-assemble to form well-defined micelles when placed in a selective solvent, i.e. a good solvent for only one of the blocks.[1,2] Typically, this is achieved by dissolving the diblock copolymer chains in a good solvent for both blocks, and then gradually reducing the solvency for one of the blocks to induce micellization.[3,4] This is known as the 'solvent switch' method and is typically conducted in dilute solution.[3] Generally, the most common copolymer morphology protocols from such post-polymerization processing protocols is spheres, but worms or vesicles can also be obtained.[5–8] One significant drawback of this traditional approach is that self-assembly is typically only conducted in dilute solution (0.1-1.0% w/w), which is too low for most potential commercial applications.[3]

Over the past decade, the development of polymerization-induced self-assembly (PISA) has enabled block copolymer self-assembly at much higher copolymer concentrations (up to 50 % w/w).[9–13] In PISA, a soluble homopolymer precursor is prepared using a controlled radical polymerization technique such as reversible addition-fragmentation chain transfer (RAFT) polymerization. [14–16] This homopolymer is then chain-extended using a second monomer and the solvent is selected such that the growing second block becomes insoluble at some critical degree of polymerization (DP).[17] This drives in situ self-assembly of the copolymer chains to form diblock copolymer nanoparticles, with the final copolymer morphology often depending solely on the relative volume fractions of the soluble and insoluble blocks.[18] In practice, other synthesis parameters such as the DP of the soluble block,[19] the topology of the soluble block[20] and the overall copolymer concentration can also play important roles.[21] In particular, it is well-known that some PISA formulations only lead to the formation of kinetically-trapped spheres even when highly asymmetric diblock copolymer compositions are targeted.[22–24]

Poly(benzyl methacrylate) (PBzMA) has been widely used as a core-forming block for many PISA syntheses, including RAFT aqueous emulsion polymerization,[25–27] RAFT alcoholic dispersion polymerization,[28–31] and RAFT dispersion polymerization in various non-polar solvents, including *n*-heptane,[32] *n*-dodecane,[33] mineral oil and poly(α-olefins).[34] For the former PISA formulations, kinetically-trapped spheres were observed when using either non-ionic[25] or anionic steric stabilizer[26] blocks. On the other hand, RAFT dispersion polymerization typically provides convenient access to spheres, worms or vesicles provided that the steric stabilizer block is chosen to be sufficiently short to allow efficient sphere-sphere fusion to occur on the time scale of the polymerization.[23]

Recently, we reported that the RAFT dispersion polymerization of various methacrylic monomers can be conducted in decamethylcyclopentasiloxane (D5), which is a low-viscosity silicone oil.[35] More specifically, a monohydroxy-functionalized $PDMS_{66}$ precursor was esterified with a carboxylic acid-functionalized, trithiocarbonate-based RAFT agent. The resulting $PDMS_{66}$ precursor was chain-extended using eight different methacrylic monomers in turn. However, only spheres could be obtained when using BzMA for the core-forming block and six other monomers yielded the same kinetically-trapped morphology. Exceptionally, using 2-(dimethylamino)ethyl methacrylate (DMA) allowed access to spheres, worms or vesicles. This was attributed to the relatively low glass transition temperature (T_g) for poly(2-(dimethylamino)ethyl methacrylate), which confers greater chain mobility. This is believed to be important for worm formation via stochastic 1D fusion of multiple spheres.[36]

The observation of kinetically-trapped $PDMS_{66}$-$PBzMA_x$ spheres in D5 was particularly surprising because precisely the same PISA system produces spheres, worms or vesicles when using *n*-heptane.[37] It is widely recognized that, if a particular RAFT dispersion polymerization formulation is limited to kinetically-trapped spheres, reducing the molecular weight of the steric stabilizer block usually enables access to worms or vesicles.[33,38] However, rather few monohydroxy-capped PDMS

precursors are commercially available, so this approach is not convenient for the PDMS-PBzMA$_x$ system.

In the present study, we replace the PDMS stabilizer block with poly(3-[tris(trimethylsilyloxy)silyl] propyl methacrylate) (PSiMA). This silicone-based methacrylic polymer is readily prepared by RAFT solution polymerization of SiMA in toluene (see **Scheme 1**). By targeting relatively short stabilizer DPs, we examine whether spheres, worms and vesicles can be accessed when targeting PSiMA-PBzMA diblock copolymer nano-objects in D5.

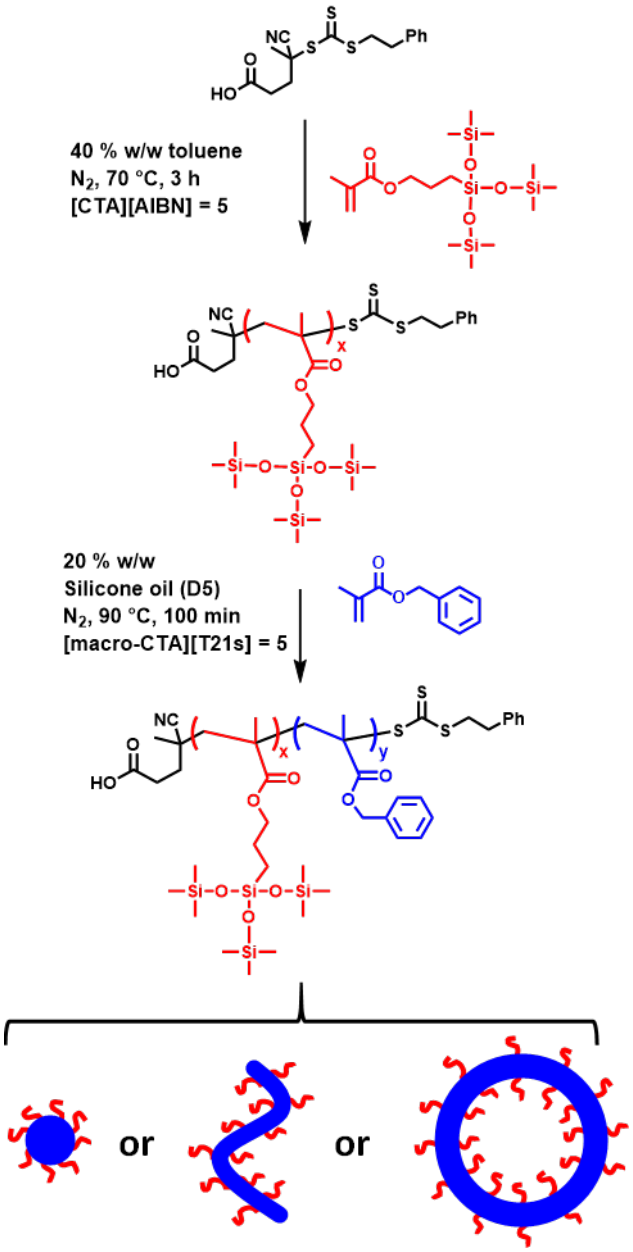

Scheme 1. Reaction scheme for the synthesis of a series of $PSiMA_x$ precursors (where x = 12, 13 or 15) via RAFT solution polymerization of SiMA in toluene using PETTC as a RAFT agent at 70 °C. Such $PSiMA_x$ precursors were then chain-extended using BzMA in D5 at 90 °C to produce 20 % w/w dispersions of $PSiMA_x$-$PBzMA_y$ diblock copolymer nano-objects.

Experimental section

Materials

SiMA was purchased from Alfa Aesar (USA) and used as received. BzMA, butylated hydroxytoluene (BHT), trimethylamine, methanol, toluene, 2,2'-azobisisobutyronitrile (AIBN) and tetrahydrofuran (THF) were purchased from Sigma Aldrich (UK) and used as received. 4-Cyano-4-(2-phenylethanesulfanylthiocarbonyl)sulfanylpentanoic acid (PETTC) RAFT agent was prepared according to a previously described protocol.[27] Trigonox 21s (T21s) initiator was obtained from AkzoNobel (The Netherlands) and used as received. D5 silicone oil was obtained from the Scott Bader Company Ltd. (UK) and used as received. $CDCl_3$ and CD_2Cl_2 were purchased from Goss Scientific (UK) and used as received.

4.2.2 Methods

Synthesis of PSiMA precursors

A typical synthesis of a $PSiMA_{12}$ precursor was conducted as follows: PETTC (2.46 g, 7.26 mmol), SiMA monomer (36.7 g, 86.9 mmol) and toluene (59.1 g) were added to a round-bottomed flask in order to target a PSiMA DP of 12. AIBN was then added (23.8 mg, 1.44 mmol; [PETTC]/[AIBN] = 5.0). The resulting mixture was sealed, purged with nitrogen, and the round-bottomed flask was placed in a preheated oil bath set at 70 °C for 3 h. The polymerization was then quenched by simultaneously cooling the reaction mixture in an ice bath and exposing it to air. ^{1}H NMR spectroscopy studies indicated a SiMA conversion of 67 %. The crude PSiMA was purified by precipitation into a ten-fold excess of 95:5 % v/v methanol/water (three times) before being dissolved in *n*-hexane (100 mL), washed with saturated aqueous sodium chloride (3 x 100 mL) and dried over magnesium sulfate. The resulting solution was then filtered and placed under reduced pressure to remove the *n*-hexane,

enabling a purified $PSiMA_{12}$ precursor to be isolated. ^{1}H NMR spectra recorded in CD_2Cl_2 indicated a mean PSiMA DP of 12, by comparing the oxymethylene protons at 3.9 ppm assigned to the PSiMA block with the five aromatic protons assigned to the PETTC chain-ends at 7.3 ppm. THF GPC analysis indicated an M_n of 3900 g mol^{-1} and an M_w/M_n of 1.12. This protocol was also used to prepare two other $PSiMA_x$ precursors with mean DPs of either 13 or 15.

Synthesis of $PSiMA_{12}$-$PBzMA_x$ nanoparticles via RAFT dispersion polymerization of BzMA in D5

$PSiMA_y$-$PBzMA_x$ (where x = 12, 13 or 15, and y was varied between 20 and 200) nanoparticles were synthesized *via* RAFT dispersion polymerization of BzMA in D5 silicone oil. A typical synthesis targeting $PSiMA_{15}$-$PBzMA_{180}$ was conducted as follows: $PSiMA_{15}$ precursor was weighed out into a 10 ml vial (0.10 g, 15 µmol). To this, D5 silicone oil (2.30 g) was added, along with benzyl methacrylate (0.48 g, 2.70 mmol) to afford a target PBzMA DP of 180 and a final copolymer concentration of 20 % w/w. Next, T21s initiator was added (3.75 µmol, 9 µl; added as a 10 % v/v solution in D5) along with a magnetic stirrer bar. The resulting mixture was then sealed and purged with nitrogen gas for 20 min, before being placed in a preheated oil bath set at 90 °C for 5 h. ^{1}H NMR spectroscopy studies performed in $CDCl_3$ indicated BzMA conversions of 90 – 99 % were achieved in all cases. Furthermore, THF GPC analysis confirmed low dispersities (M_w/M_n < 1.25) for each diblock copolymer.

4.2.3 Characterization

^{1}H NMR spectroscopy

^{1}H NMR spectra were recorded in either CD_2Cl_2 or $CDCl_3$ using a Bruker AV1-400 MHz spectrometer. Typically, 64 scans were averaged per spectrum.

Gel permeation chromatography

Molecular weight distributions were determined using a GPC set-up operating at 30 °C that comprised two Polymer Laboratories PL gel 5 µm Mixed C columns, a LC20AD ramped isocratic pump,

THF eluent and a WellChrom K-2301 refractive index detector operating at 950 ± 30 nm. The mobile phase contained 2.0 % v/v triethylamine and 0.05 % w/v 3,5-di-tert-4-butylhydroxytoluene (BHT); the flow rate was 1.0 ml min^{-1}. A series of ten near-monodisperse poly(methyl methacrylate) standards (M_n = 1 280 to 330 000 g mol^{-1}) were used for calibration. Chromatograms were analyzed using Varian Cirrus GPC software.

Dynamic light scattering

Dynamic light scattering (DLS) studies were performed using a Zetasizer Nano-ZS instrument (Malvern Instruments, UK) at 25 °C at a fixed scattering angle of 173°. Copolymer dispersions were diluted in the solvent in which they were synthesized (typically D5) to a final concentration of 0.10 % w/w. The intensity-average diameter and polydispersity (PDI) of the diblock copolymer nanoparticles were calculated by cumulants analysis of the experimental correlation function using Dispersion Technology Software version 6.20. Data were averaged over ten runs each of thirty seconds duration.

Transmission electron microscopy

Transmission electron microscopy (TEM) studies were conducted using a FEI Tecnai G2 spirit instrument operating at 80 kV and equipped with a Gatan 1k CCD camera. Copper TEM grids were surface-coated in-house to yield a thin film of amorphous carbon. The grids were then loaded with dilute copolymer dispersions (0.20 % w/w). Prior to imaging, each grid was exposed to ruthenium(IV) vapour for 7 min at ambient temperature in order to achieve sufficient contrast. The ruthenium oxide stain was prepared by adding ruthenium(II) oxide (0.30 g) to water (50 g), to form a slurry. Then sodium periodate (2.0 g) was added to the stirred solution and a yellow solution of ruthenium(IV) oxide was formed within 1 min at 20 °C.[39]

Rheology studies

An AR-G2 rheometer equipped with a 40 mm 2° aluminum cone was used for all measurements. The storage and loss moduli were determined *via* oscillatory rheometry either as a function of strain at a fixed angular frequency of 1.0 rad s^{-1} or as a function of angular frequency at a fixed strain of 1.0 %.

Small-angle X-ray scattering

Spherical micelles. SAXS patterns were recorded at an international synchrotron facility (Diamond Light Source, station I22, Didcot, UK) using monochromatic X-ray radiation (wavelength λ = 0.124 nm, with *q* ranging from 0.015 to 1.3 nm^{-1}, where *q* is the length of the scattering vector ($q = 4\pi.\sin\theta/\lambda$) and θ is one-half of the scattering angle), and a 2D Pilatus 2M pixel detector (Dectris, Switzerland). Measurements were conducted on 1.0% w/w copolymer dispersions and glass capillaries of 2.0 mm diameter were used as a sample holder. X-ray scattering data were reduced and normalized using standard routines provided by the beamline. The data were further analyzed and modeled using Irena SAS macros for Igor Pro.[40] Further details of the spherical micelle model used for such data fits are provided in the Supporting Information.

Worm-like micelles and vesicles. SAXS patterns were recorded at a synchrotron source (ESRF, station ID02, Grenoble, France) using monochromatic X-ray radiation (wavelength λ = 0.0995 nm, with q ranging from 0.004 to 2.5 nm^{-1}) and a Rayonix MX-170HS Kodak CCD detector. Measurements were conducted on 1.0% w/w copolymer dispersions and glass capillaries of 2.0 mm diameter were used as a sample holder. X-ray scattering data were reduced and normalized using standard routines provided by the beamline. The data were further analyzed and modeled using Irena SAS macros for Igor Pro.[40] Further details of the worm and vesicle scattering models are provided in the Supporting Information.

Results and discussion

The RAFT solution polymerization of SiMA was conducted in toluene, using PETTC as the RAFT agent and AIBN as an initiator. The target copolymer concentration was fixed at 40 % w/w, and the

[PETTC]/[AIBN] molar ratio was fixed at 5.0. **Figure 1** shows typical kinetic data obtained for the RAFT solution polymerization of SiMA in toluene conducted at 70 °C when targeting a final PSiMA DP of 12. These data were obtained by removing aliquots from the polymerizing mixture at regular time intervals followed by analysis using ^{1}H NMR spectroscopy and THF GPC. An induction period of approximately 30 min was observed at the beginning of the polymerization, which is well-documented for related RAFT polymerizations.[41,42] Nevertheless, 86 % SiMA conversion was achieved within 6 h at 70 °C. Moreover, THF GPC analysis indicated a linear evolution in PSiMA molecular weight as expected for a well-controlled RAFT polymerization, while dispersities remained below 1.20 throughout. A representative ^{1}H NMR spectrum obtained for an aliquot removed from the polymerizing reaction mixture after 240 min is shown in **Figure S1**.

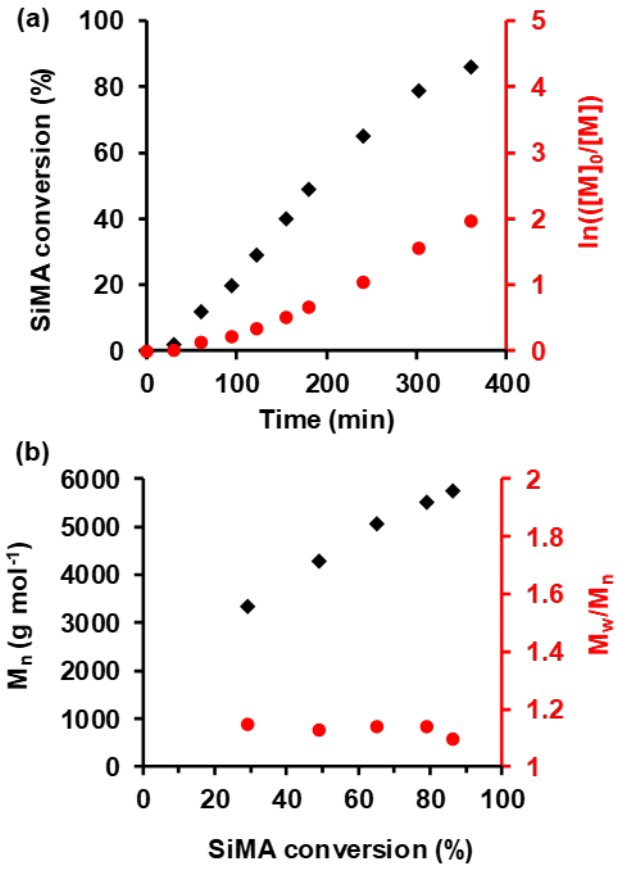

Figure 1. (a) SiMA monomer conversion vs. time curve (black diamonds) obtained for the RAFT solution polymerization of SiMA at 40 % w/w in toluene at 70 °C using PETTC as a CTA and AIBN as an initiator ([PETTC]/[AIBN] = 5.0). The PSiMA target DP was 12 and conversions were determined *via* ^{1}H NMR spectroscopy. The corresponding semi-logarithmic plot is also shown (red circles). (b) Selected THF GPC data obtained for the same polymerization. A linear evolution in M_n with SiMA

conversion was observed (black diamonds), and M_w/M_n values remained below 1.20 throughout (red circles), indicating good pseudo-living character. [N.B. Aliquots removed at SiMA conversions below 30 % could not be analyzed as elution occurred outside the GPC column calibration limit].

Based on these polymerization kinetics, three $PSiMA_x$ precursors were prepared for which x = 12, 13 or 15, as summarized in **Table 1**. In each case, polymerizations were quenched at between 60 and 80 % conversion to preserve RAFT chain-end fidelity. A typical ^{1}H NMR spectrum obtained for the $PSiMA_{12}$ precursor is shown in **Figure 2b**.

Table 1: Summary of conversion and molecular weight data obtained for three PSiMA precursors prepared via RAFT solution polymerization of SiMA at 70 °C and 40 % w/w in toluene

Precursor	Target DP	Conversion %[a]	Actual DP[b]	M_n (GPC)[c]	M_w/M_n (GPC)[c]
$PSiMA_{12}$	10	67	12	3900	1.12
$PSiMA_{13}$	11	76	13	4300	1.14
$PSiMA_{15}$	13	60	15	4800	1.12

[a] ^{1}H NMR in $CDCl_3$ [b1]^{1}H NMR in CD_2Cl_2 [c] THF GPC vs. PMMA standards

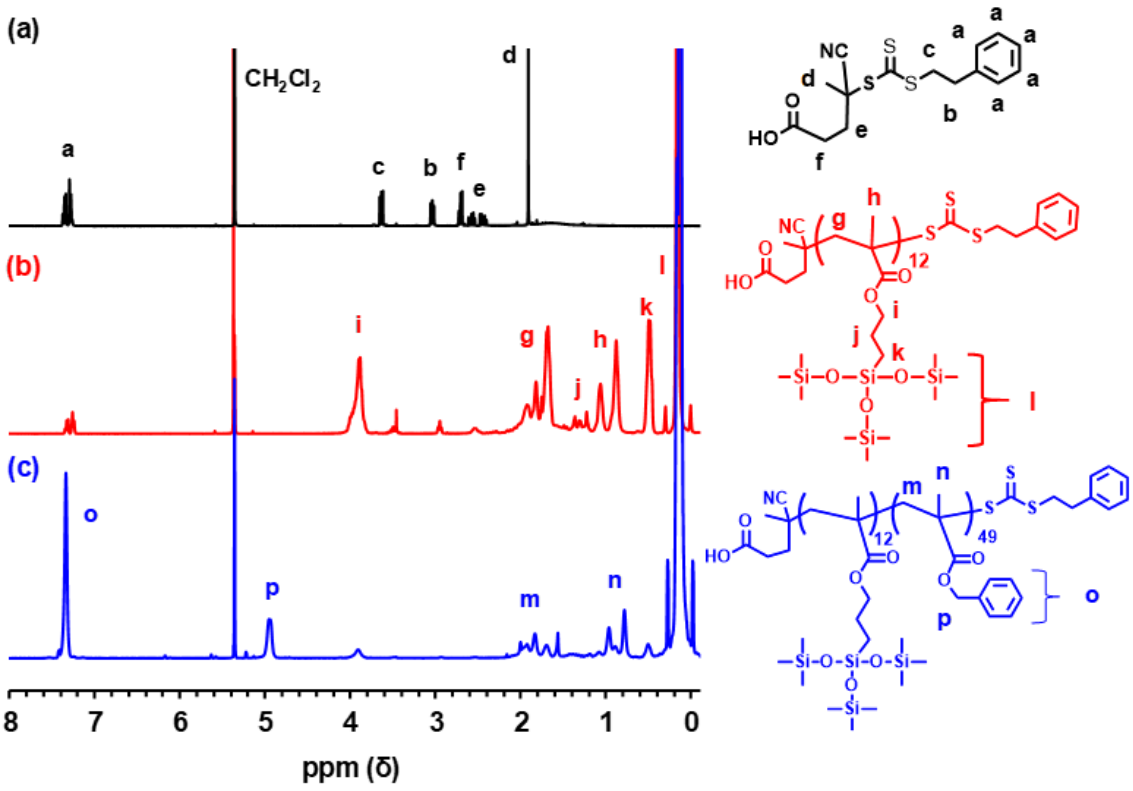

Figure 2. ^{1}H NMR spectra recorded in CD_2Cl_2 for: (a) PETTC RAFT agent, (b) a $PSiMA_{12}$ precursor and (c) a $PSiMA_{12}$-$PBzMA_{49}$ diblock copolymer prepared in D5.

The mean DP for each PSiMA precursor was determined by comparing the five aromatic protons (labeled a) at 7.3 ppm assigned to the PETTC CTA with the oxymethylene protons (labeled i) at around 3.9 ppm assigned to the polymer (see **Figure 2**). THF GPC analysis of each of these precursors indicated a unimodal molecular weight distribution in each case (see **Figure S2**) and dispersities below 1.15 (see **Table 1**).

Next, the $PSiMA_{15}$ precursor was used to polymerize BzMA via RAFT dispersion polymerization at 90°C in D5. A PBzMA core-forming DP of 200 was targeted at a final copolymer concentration of 20 % w/w. In addition, this synthesis was scaled up to 10.0 g in order to facilitate detailed kinetic studies of the BzMA polymerization (**Figure 3a**), which required removal of aliquots from the polymerizing reaction mixture at regular time intervals for subsequent analysis by ^{1}H NMR spectroscopy and THF GPC.

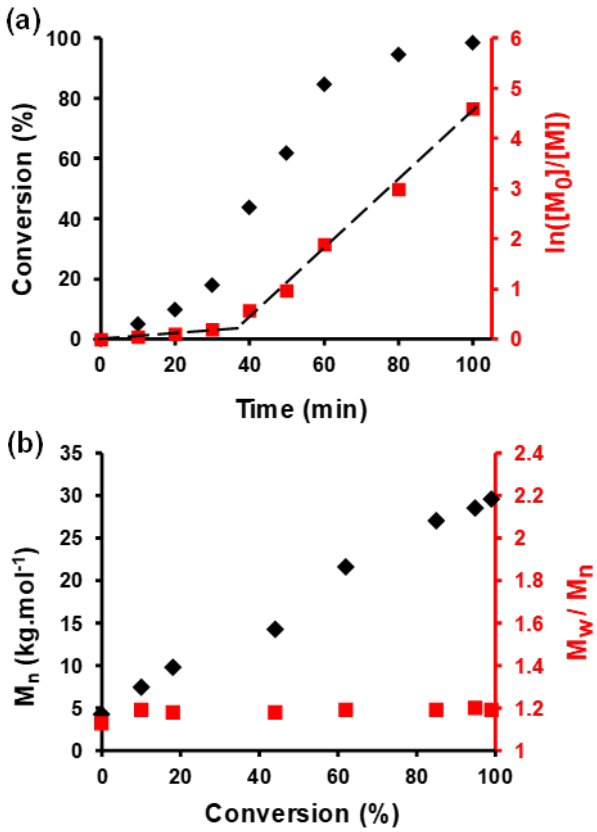

Figure 3. (a) Conversion vs. time curve (black diamonds) obtained for the polymerization of BzMA in D5 at 90 °C utilizing a $PSiMA_{15}$ precursor and Trigonox 21s (T21s) as an initiator. The copolymer concentration was fixed at 20 % w/w, the $[PSiMA_{15}]/[T21s]$ molar ratio was fixed at 4.0 and the target PBzMA DP was 200. The corresponding semi-logarithmic plot is also shown (red squares). (b)

Evolution in M_n (black diamonds) and M_w/M_n (red squares) with BzMA conversion as determined by THF GPC analysis of aliquots taken from the same kinetic run shown in (a).

The initial solution polymerization proceeded relatively slowly for the first 30 min. Thereafter, an eleven-fold rate enhancement was observed (**Figure 3a**), which coincided with the initial transparent reaction mixture becoming turbid. This is observed for many PISA formulations, and is attributed to the onset of nucleation.[36,43] Initially, the polymerization takes place under homogeneous conditions until a critical PBzMA DP is achieved, after which this block becomes insoluble in D5 and micellization occurs. The growing PBzMA chains within the nascent micelle cores are solvated by unreacted BzMA monomer, which results in a higher local monomer concentration and hence a significantly faster rate of reaction.[36] Thus the monomer acts as a highly convenient co-solvent to aid processing. Overall, more than 99 % BzMA conversion was achieved within 100 min at 90 °C. THF GPC analysis indicated a linear evolution in M_n with monomer conversion while M_w/M_n values remained below 1.22 throughout, as expected for a well-controlled RAFT polymerization (see **Figure 3b**). Furthermore, each chromatogram was unimodal, indicating efficient chain extension of the $PSiMA_{15}$ precursor chains (see **Figure S3**).

Each of the three PSiMA precursors were chain-extended in turn with BzMA in D5 at 20% w/w solids in order to construct a phase diagram (see **Figure 4**).

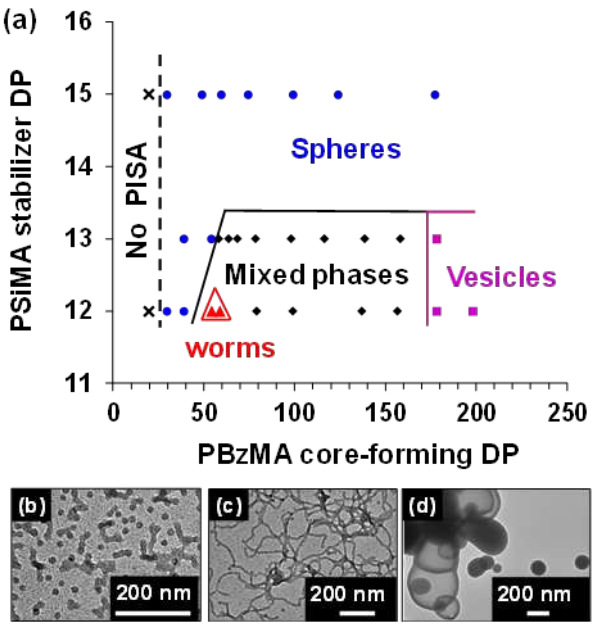

Figure 4. (a) Phase diagram obtained for the RAFT dispersion polymerization of BzMA at 90 °C in D5 at 20 % w/w using a $PSiMA_x$ precursor (where x = 12, 13 or 15). In each case the copolymer morphology was assigned based on combined TEM and DLS studies, where w denotes worms. Representative TEM images are also shown for: (b) $PSiMA_{12}$-$PBzMA_{40}$ spheres, (c) $PSiMA_{12}$-$PBzMA_{55}$ worms and (d) $PSiMA_{12}$-$PBzMA_{200}$ vesicles.

The polymers used to construct this phase diagram, along with characterization data, are outlined in **Table S1**. For a fixed PSiMA DP of 15, well-defined spherical nanoparticles were obtained when targeting core-forming PBzMA DPs of between 30 and 180, as determined by TEM. DLS analysis indicated that such spheres had z-average diameters ranging between 19 nm and 49 nm. Moreover, THF GPC analysis indicated that each polymerization was well-controlled, with low dispersities and high blocking efficiencies being observed in each case. **Figure 5a** shows a double-logarithmic plot of z-average diameter against the DP of the core-forming PBzMA block.

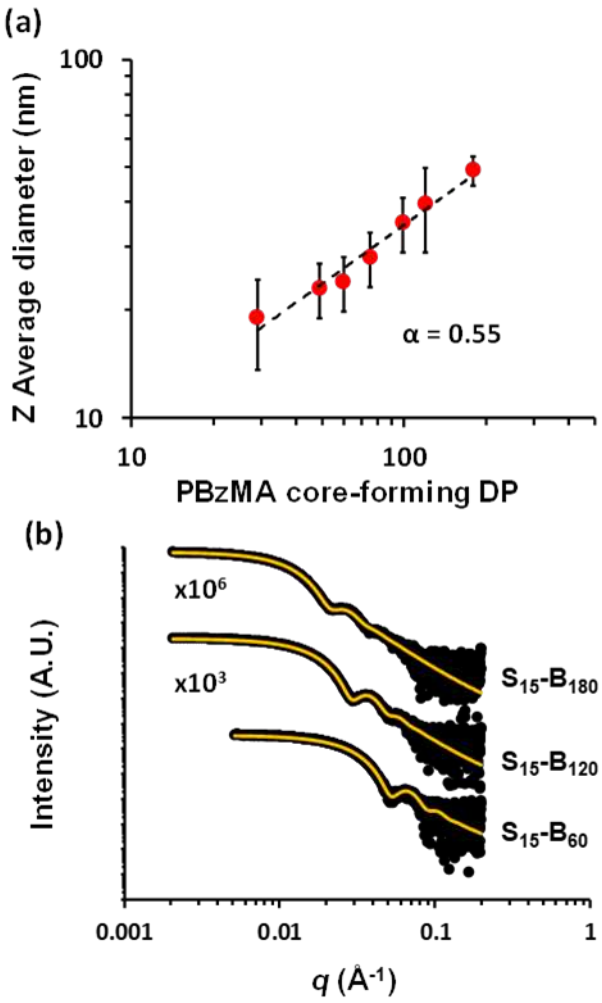

Figure 5. (a) Z-average diameter determined by DLS (recorded at 0.1 % w/w copolymer concentration in D5) vs. PBzMA core-forming DP, obtained for a series of $PSiMA_{15}$-$PBzMA_x$ spherical nanoparticles. (b) SAXS patterns (black data; recorded at 1.0 % w/w solids in D5) obtained for a series of $PSiMA_{15}$-$PBzMA_x$ spherical nanoparticles. For brevity, S denotes PSiMA and B denotes PBzMA. The data fits, shown as amber lines, were obtained using a spherical micelle model. For clarity, the patterns obtained for S_{15}-B_{120} and S_{15}-B_{180} are offset by factors of 10^3 and 10^6, respectively.

As expected for such PISA-synthesized spheres, this relationship is linear and can be fitted using the power law relation, $D \sim k.x^{\alpha}$.[44] Here, D is the mean sphere diameter, x is the PBzMA DP, k is an arbitrary constant and α is the scaling exponent. For the $PSiMA_{15}$-$PBzMA_x$ series we find that α = 0.55, which lies roughly between the weak segregation limit and strong segregation limit. This value is consistent with those reported for various similar sterically-stabilized diblock copolymer nanoparticles (a.k.a. micelles).[23,44–46]

To obtain more robust structural characterization, three examples of apparently pure $PSiMA_{15}$-PBzMAx spheres (as judged by TEM) were selected for synchrotron SAXS analysis at Diamond Light Source (see **Figure 5b**). Each pattern could be well-fitted using a spherical micelle model, which confirmed the spherical morphology of each copolymer dispersion.[47] Moreover, the volume-average diameter of the nanoparticles increased from 20 to 35 to 47 nm on increasing the PBzMA core-forming DP from 60 to 120 to 180, respectively.

It is well-documented in the PISA literature that when the molecular weight of the steric stabilizer block is too large, kinetically-trapped spheres are the only accessible copolymer morphology.[32,48] Therefore, the DP of the PSiMA stabilizer was reduced in order to target worms and vesicles. When chain-extending a $PSiMA_{13}$ precursor with BzMA at a copolymer concentration of 20 % w/w, spheres were observed when targeting PBzMA DPs below 50 while vesicles were obtained when targeting a PBzMA DP above 170. However, only mixed phases were obtained for intermediate core-forming block DPs, i.e. no pure worm phase could be identified (see **Figure 4a**). To address this problem, the PSiMA DP was further reduced to 12. The full range of copolymer morphologies could be accessed when using this shorter $PSiMA_{12}$ stabilizer block. Thus, spheres were formed at a PBzMA DP of 40 or

below. For PBzMA DPs between 55 and 60, pure worms were produced in the form of transparent, free-standing gels. Finally, vesicles were obtained as turbid free-flowing dispersions when targeting PBzMA DPs above 170.

Next, the same $PSiMA_{12}$ precursor was used to polymerize BzMA for copolymer concentrations ranging between 5 and 20 % w/w in order to investigate the influence of this parameter on the final copolymer morphology and hence construct a second phase diagram (see **Figure 6**).

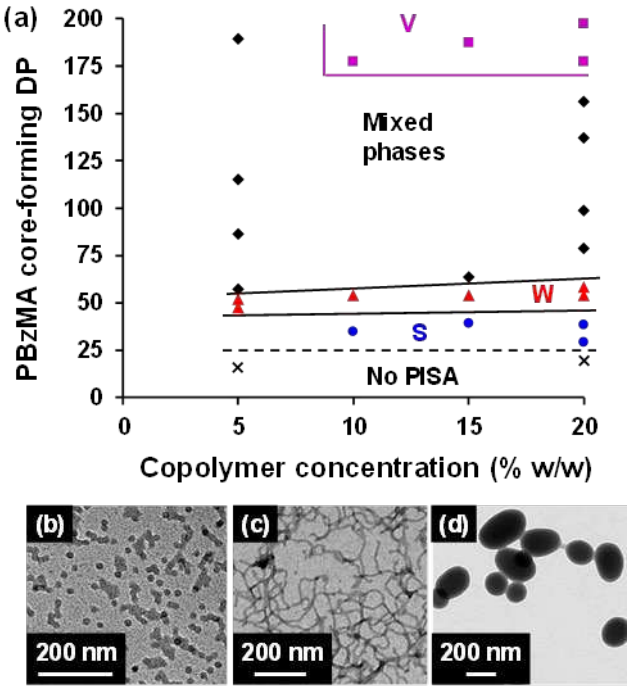

Figure 6. (a) Phase diagram obtained for the RAFT dispersion polymerization of BzMA at 90 °C in D5, using a $PSiMA_{12}$ precursor to target copolymer concentrations ranging between 5% w/w and 20% w/w. In each case, the final copolymer morphology was assigned based on combined TEM and DLS studies (V = vesicles, W = worms and S = spheres). Representative TEM images are also shown for (b) $PSiMA_{12}$-$PBzMA_{35}$ spheres, (c) $PSiMA_{12}$-$PBzMA_{55}$ worms and (d) $PSiMA_{12}$-$PBzMA_{180}$ vesicles (all prepared at 10 % w/w).

Irrespective of copolymer concentration, no PISA was observed when the PBzMA core-forming target DP was below 20. Clearly, below this critical value the PBzMA block is not sufficiently insoluble in D5 to induce micellar aggregation. Again, similar observations are well-documented in the PISA literature.[36] Perhaps surprisingly, pure vesicles could be accessed at copolymer concentrations as

low as 10% w/w while pure worms were obtained as free-standing gels at copolymer concentrations as low as 5% w/w. This is somewhat unusual for PISA syntheses performed in non-polar solvents, which often require concentrations higher than 10 % w/w to form worms.[24,48,49]

In order to obtain further structural information such as the mean aggregation number (N_{agg}), copolymer dispersions of pure spheres, worms and vesicles (as judged by TEM) were further characterized using synchrotron SAXS (see **Figure 7**). It is perhaps noteworthy that an intense X-ray source was essential for characterization of these diblock copolymer nano-objects because of the relatively high background scattering exhibited by the silicone oil.

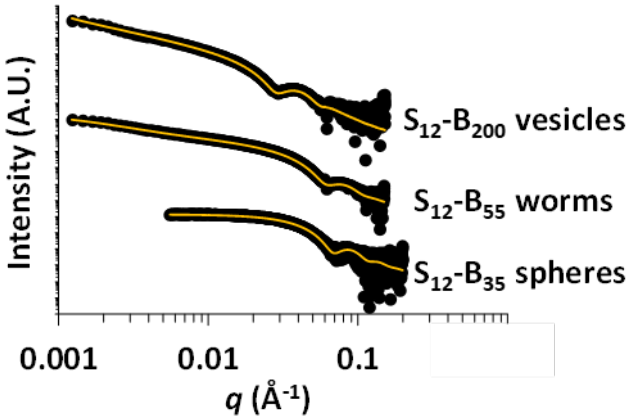

Figure 7. SAXS patterns (black data; recorded at 1.0% w/w solids in D5) obtained for (i) $PSiMA_{12}$-$PBzMA_{35}$ spherical nanoparticles, (ii) $PSiMA_{12}$-$PBzMA_{55}$ worms and (iii) $PSiMA_{12}$-$PBzMA_{200}$ vesicles, initially prepared at 10% w/w solids in D5 in each case. For brevity, S denotes PSiMA and B denotes PBzMA. Data fits are shown as amber lines and were obtained using a spherical micelle, a worm-like micelle or a vesicle model, respectively. For clarity, the patterns obtained for S_{12}-B_{55} and S_{12}-B_{200} have been offset by factors of 10 and 10^6, respectively.

A gradient of approximately zero was observed at low *q* for $PSiMA_{12}$-$PBzMA_{35}$ nanoparticles prepared at 10 % w/w, which indicates a spherical morphology. Moreover, this scattering pattern can be satisfactorily fitted using a spherical micelle model,[47] which indicates a volume-average diameter of 16 nm; this is consistent with the z-average diameter of 18 nm determined by DLS. For the $PSiMA_{12}$-$PBzMA_{55}$ nanoparticles prepared at 10% w/w in D5, a gradient of approximately -1 can be determined from the corresponding scattering pattern, which is characteristic of rod-like (and, to a good approximation, worm-like) particles.[23] Moreover, this pattern can be fitted using a worm-like

micelle model.[47] Such data analysis indicates that the worms have a mean cross-sectional diameter of 14 nm, a mean contour length of 1.6 µm, a Kuhn length of 72 nm and a mean N_{agg} of 12 400. Finally, the scattering pattern recorded for the $PSiMA_{12}$-$PBzMA_{200}$ nano-objects exhibits a gradient of approximately -2 at low *q*, which is consistent with a vesicular morphology.[23] Moreover, the data fit is consistent with a vesicle model,[50] which suggests an overall vesicle diameter of 287 nm, a membrane thickness of 22 nm and an N_{agg} of 93 353. A summary of each of the parameters calculated from the above three SAXS models is provided in **Table S2**.

In order to assess the physical properties of a 5% w/w $PSiMA_{12}$-$PBzMA_{55}$ worm gel in D5, oscillatory rheology studies were performed using a cone-and-plate geometry. First, a strain sweep was conducted at an angular frequency of 1.0 rad s^{-1} (see **Figure 8a**).

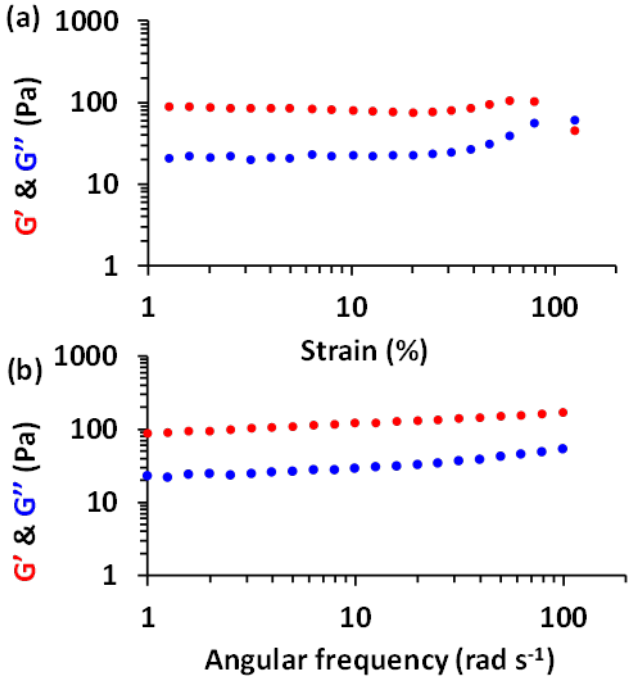

Figure 8. Oscillatory rheology studies conducted on a $PSiMA_{12}$-$PBzMA_{54}$ worm gel at 5% w/w in D5: (a) strain-sweep plot recorded at a fixed angular frequency of 1.0 rad s^{-1}, (b) frequency sweep recorded at a fixed applied strain of 1.0 %.

For small deformations (less than 25 %), both the storage and loss moduli remained independent of the applied strain, indicating the linear viscoelastic region. A yield point is observed at larger applied

strains (~ 100 %), above which G' falls below G''. Presumably, this indicates loss of the percolating worm network under such conditions.[51] Next, a frequency sweep was conducted between 1 and 100 rad s^{-1} at a constant strain amplitude of 1.0 % on a fresh worm gel. Inspecting **Figure 8b** the storage modulus (G') exceeds the loss modulus (G'') over the entire frequency range, indicating that this copolymer dispersion is indeed a gel. In addition, G' and G'' are almost independent of the applied frequency, which indicates gel-like behaviour (albeit with some viscous character). Finally, the overall magnitude of G' is approximately 100 Pa, which is relatively high given that the copolymer concentration is only 5% w/w. This indicates that these worm gels are somewhat stronger than many other worm gels prepared via PISA.[38,52]

SiMA was originally selected for the steric stabilizer block in this study because this methacrylic monomer contains no labile Si-O-R or Si-OH groups. Therefore, these nanoparticles were expected to be chemically inert and remain colloidally stable indefinitely. However, GPC studies indicated that the initial molecular weight distribution (MWD) obtained for spheres or worms broadened markedly and shifted to higher molecular weight during the long-term storage of such dispersions at ambient temperature. These observations are illustrated in **Figure 9**, which shows GPC curves recorded for 10% w/w dispersions of $PSiMA_{12}$-$PBzMA_{35}$ spheres or $PSiMA_{12}$-$PBzMA_{55}$ worms after being stored as concentrated dispersions for eight weeks at 20 °C. In contrast, no discernible change in the molecular weight distribution was observed for the analogous $PSiMA_{12}$-$PBzMA_{180}$ vesicles.

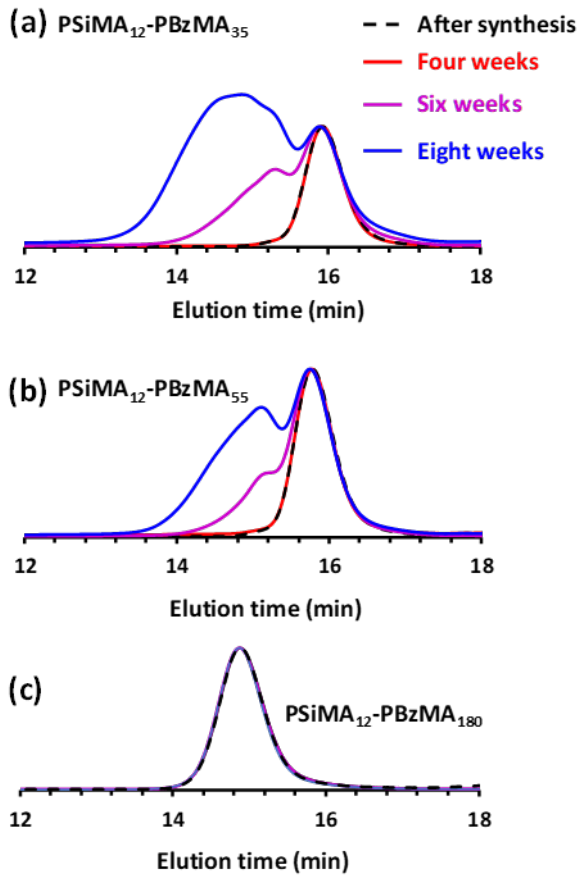

Figure 9. GPC curves recorded for (a) $PSiMA_{12}$-$PBzMA_{35}$ spheres, (b) $PSiMA_{12}$-$PBzMA_{55}$ worms and (c) $PSiMA_{12}$-$PBzMA_{180}$ during the long-term storage of such concentrated dispersions at 20°C. In each case, measurements were conducted directly after each PISA synthesis (black dashed line), after four weeks (red trace), after six weeks (purple trace) and after eight weeks (blue trace).

In all three cases, relatively little change in the MWD was observed over the first four weeks after synthesis. However, for the spheres and worms, a distinct shoulder was observed after 6 weeks, indicating the onset of light crosslinking between copolymer chains. This feature became much more pronounced after eight weeks. This suggests that some kind of side-reaction occurs at ambient temperature. The commercial grade of SiMA monomer used in this study is known to contain a minor fraction of Si-OH impurity. If such silanol species are present, condensation reactions between neighbouring PSiMA stabilizer chains could lead to crosslinking between neighboring copolymer chains *within* nanoparticles (see **Scheme S1**). Nevertheless, the MWD recorded for the $PSiMA_{12}$-$PBzMA_{180}$ vesicles remained unchanged after eight weeks, suggesting that no crosslinking occurredin

this particular case. One plausible explanation for this apparent discrepancy is that the $PSiMA_{12}$-$PBzMA_{180}$ vesicles contain a significantly lower molar concentration of $PSiMA_{12}$ (2.9 mmol dm^{-3}) compared with either $SiMA_{12}$-$PBzMA_{35}$ spheres (9.2 mmol dm^{-3}) or $PSiMA_{12}$-$PBzMA_{55}$ worms (7.0 mmol dm^{-3}).

In principle, such crosslinking can also occur *between* nanoparticles, which would be expected to lead to their aggregation. To examine whether this side-reaction also affects the long-term colloidal stability of such copolymer dispersions, DLS studies were performed at the same time as the GPC experiments. (see **Figure 10**). For the $PSiMA_{12}$-$PBzMA_{35}$ spheres, DLS analysis of a 0.1% w/w dispersion prepared directly after the PISA synthesis indicated a z-average diameter of 19 nm and a corresponding polydispersity index (PDI) of 0.01. DLS analysis conducted after four weeks indicated a z average diameter of 19 nm and a similar PDI of 0.04, suggesting that these nanoparticles remained colloidally stable over this time period. After six weeks, the z-average diameter remained almost unchanged at 20 nm but the PDI had increased up to 0.16. This suggests that incipient flocculation has occurred via *interparticle* crosslinking. Similar DLS observations were made for the $PSiMA_{12}$-$PBzMA_{55}$ worms. However, it is important to note here that such DLS experiments rely on the Stokes-Einstein equation, which assumes a spherical morphology. Consequently, for highly anisotropic worms, DLS simply reports the 'sphere-equivalent' hydrodynamic diameter, which does not correspond to either the mean worm length or width.[33] Nevertheless, DLS can be used to detect *relative* changes in the worm dimensions. Thus, the DLS size distribution recorded for the as-synthesized $PSiMA_{12}$-$PBzMA_{55}$ worms overlaid perfectly with that obtained for the same worms after four weeks storage at 20°C. This indicates that such worms are colloidally stable for at least four weeks, which is consistent with the GPC analysis.

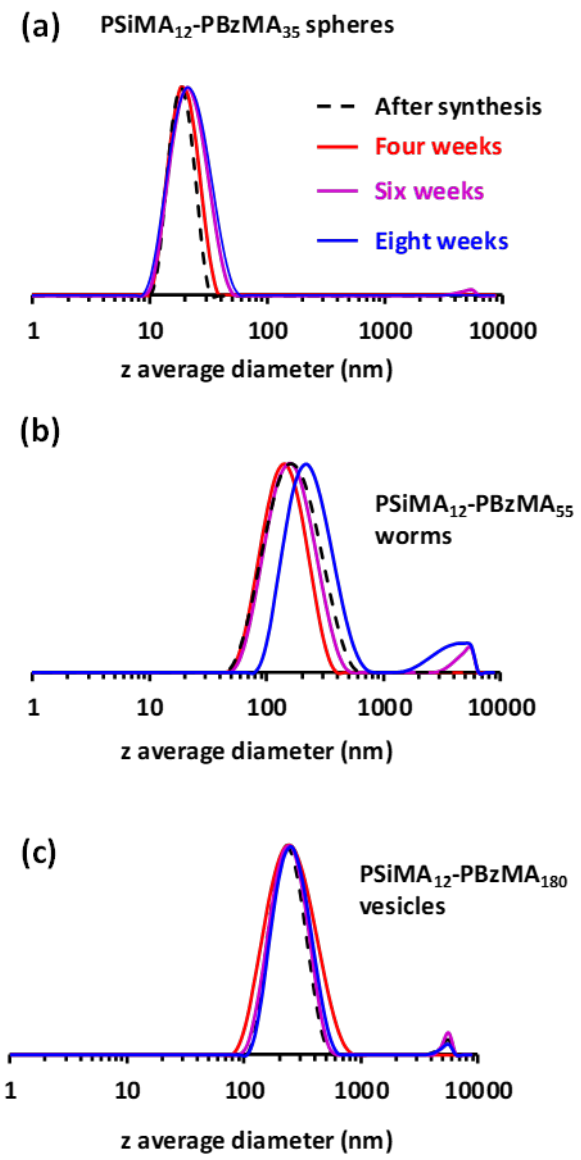

Figure 10. DLS data recorded for 0.1% w/w dispersions of (a) $PSiMA_{12}$-$PBzMA_{35}$ spheres, (b) $PSiMA_{12}$-$PBzMA_{55}$ worms and (c) $PSiMA_{12}$-$PBzMA_{180}$ in silicone oil during the long-term storage of such concentrated dispersions at 20°C. In each case, measurements were conducted directly after each PISA synthesis (black dashed line), after four weeks (red trace), after six weeks (purple trace) and after eight weeks (blue trace).

However, the six-week aged $PSiMA_{12}$-$PBzMA_{55}$ worm gel proved to be significantly harder to dilute using silicone oil. This is consistent with the onset of inter-worm crosslinking, which would be expected to retard dissociation of the 3D network of inter-connected worms.[51] Moreover, a bimodal size distribution was observed by DLS, with a minor population within the micron size range. After eight weeks storage at 20°C, a significant shift in the 'sphere-equivalent' hydrodynamic diameter

from 122 nm to 210 nm was observed. Moreover, the larger population became more prominent, which suggests the formation of micron-sized aggregates via inter-worm crosslinking. In contrast, very little change in the initial DLS size distribution was observed for the $PSiMA_{12}$-$PBzMA_{180}$ vesicles over eight weeks at 20°C. This is consistent with the above GPC analysis of this dispersion.

Conclusions

A series of well-defined $PSiMA_x$ homopolymers (where x = 12, 13 or 15) were prepared by the RAFT solution polymerization of SiMA. Each of these precursors was then chain-extended in turn via RAFT dispersion polymerization of BzMA at 20% w/w solids in a silicone oil (D5) and two phase diagram were constructed for these PISA formulations. Only kinetically-trapped spheres could be obtained when utilizing the $PSiMA_{15}$ block, even when targeting relatively long PBzMA core-forming blocks. Nevertheless, such spheres are well-defined with mean z-average diameters ranging between 19 nm and 49 nm, as determined by DLS. When utilizing a relatively short $PSiMA_{12}$ precursor, either spheres, worms or vesicles can be accessed depending on the PBzMA core-forming DP. Moreover, $PSiMA_{12}$-$PBzMA_x$ worms can be synthesized at copolymer concentrations as low as 5% w/w. Selected spheres, worms and vesicles were further characterized by SAXS to determine mean diameters, mean worm cross-section diameters and persistence lengths, and mean vesicle membrane thicknesses. $PSiMA_{12}$-$PBzM_{54}$ worms were selected for further study by oscillatory rheology to assess their gelation behavior. Such worms formed relatively transparent free-standing gels at copolymer concentrations as low as 5% w/w with a G' of 90 Pa. Finally, $PSiMA_{12}$-$PBzMA_{35}$ spheres and $PSiMA_{12}$-$PBzMA_{55}$ worms became gradually cross-linked and flocculated when stored for eight weeks at ambient temperature. This unexpected long-term instability is tentatively attributed to condensation side-reactions occurring between a minor fraction of hydroxyl-functional SiMA repeat units.

Acknowledgments We thank EPSRC for a CDT PhD studentship for M.J.R. (EP/ L016281) and the Scott Bader Company Ltd. for CASE support of this project and for permission to publish these results. S.P.A. acknowledges an EPSRC Particle Technology Fellowship grant (EP/R003009). The authors thank Christopher Hill and Dr. Svetomir Tzokov at the University of Sheffield Biomedical Science Electron Microscopy suite. Also, we are grateful to the European Synchrotron Radiation Facility and Diamond Light Source for providing beam time at the ID02 beamline (ESRF, SC-4864) and I22 beamline (Diamond, SM19852).

Supporting Information Available Additional ^{1}H NMR spectra and GPC chromatograms. Tabulated block copolymer characterization data and nanoparticle structural parameters obtained from SAXS data fitting. Details of the SAXS sphere, worm and vesicle models.

Author ORCID IDs

Steven P. Armes: 0000-0002-8289-6351

Matthew J. Rymaruk: 0000-0002-6622-6251

References

(1) Krause, S. Dilute Solution Properties of a Styrene—Methyl Methacrylate Block Copolymer. *J. Phys. Chem.* **1964**, *68*, 1948–1955.

(2) Blanazs, A.; Armes, S. P.; Ryan, A. J. Self-Assembled Block Copolymer Aggregates: From Micelles to Vesicles and Their Biological Applications. *Macromol. Rapid Commun.* **2009**, *30*, 267–277.

(3) Mai, Y.; Eisenberg, A. Self-Assembly of Block Copolymers. *Chem. Soc. Rev.* **2012**, *41*, 5969–5985.

(4) Zhang, L.; Eisenberg, A. Multiple Morphologies of "Crew-Cut" Aggregates of Polystyrene-b-Poly(Acrylic Acid) Block Copolymers. *Science* **1995**, *268*, 1728–1731.

(5) Won, Y.-Y.; Davis, H. T.; Bates, F. S. Giant Wormlike Rubber Micelles. *Science* **1999**, *283*, 960–963.

(6) Antonietti, M.; Förster, S. Vesicles and Liposomes: A Self-Assembly Principle Beyond Lipids.

Adv. Mater. **2003**, *15*, 1323–1333.

(7) Discher, D. E.; Eisenberg, A. Polymer Vesicles. *Science* **2002**, *297*, 967–973.

(8) Zhang, L.; Yu, K.; Eisenberg, A. Ion-Induced Morphological Changes in ``Crew-Cut'' Aggregates of Amphiphilic Block Copolymers. *Science* **1996**, *272*, 1777–1779.

(9) Ferguson, C. J.; Hughes, R. J.; Nguyen, D.; Pham, B. T. T.; Gilbert, R. G.; Serelis, A. K.; Such, C. H.; Hawkett, B. S. Ab Initio Emulsion Polymerization by RAFT-Controlled Self-Assembly [§]. *Macromolecules* **2005**, *38*, 2191–2204.

(10) Charleux, B.; Delaittre, G.; Rieger, J.; D'Agosto, F. Polymerization-Induced Self-Assembly: From Soluble Macromolecules to Block Copolymer Nano-Objects in One Step. *Macromolecules* **2012**, *45*, 6753–6765.

(11) Warren, N. J.; Armes, S. P. Polymerization-Induced Self-Assembly of Block Copolymer Nano-Objects via RAFT Aqueous Dispersion Polymerization. *J. Am. Chem. Soc.* **2014**, *136*, 10174–10185.

(12) Canning, S. L.; Smith, G. N.; Armes, S. P. A Critical Appraisal of RAFT-Mediated Polymerization-Induced Self-Assembly. *Macromolecules* **2016**, *49*, 1985–2001.

(13) Pei, Y.; Lowe, A. B.; Roth, P. J. Stimulus-Responsive Nanoparticles and Associated (Reversible) Polymorphism via Polymerization Induced Self-Assembly (PISA). *Macromol. Rapid Commun.* **2017**, *38*, 1–14.

(14) Chiefari, J.; Chong, Y. K. B.; Ercole, F.; Krstina, J.; Jeffery, J.; Le, T. P. T.; Mayadunne, R. T. A.; Meijs, G. F.; Moad, C. L.; Moad, G.; et al. Living Free-Radical Polymerization by Reversible Addition−Fragmentation Chain Transfer: The RAFT Process. *Macromolecules* **1998**, *31*, 5559–5562.

(15) Moad, G.; Rizzardo, E.; Thang, S. H. Toward Living Radical Polymerization. *Acc. Chem. Res.* **2008**, *41*, 1133–1142.

(16) Moad, G.; Rizzardo, E.; Thang, S. H. Living Radical Polymerization by the RAFT Process—A First Update. *Aust. J. Chem.* **2006**, *59*, 669–692.

(17) Penfold, N. J. W.; Yeow, J.; Boyer, C.; Armes, S. P. Emerging Trends in Polymerization-Induced Self-Assembly. *ACS Macro Lett.* **2019**, *8*, 1029–1054.

(18) Lowe, A. B. RAFT Alcoholic Dispersion Polymerization with Polymerization-Induced Self-Assembly. *Polymer* **2016**, *106*, 161–181.

(19) Busatto, N.; Stolojan, V.; Shaw, M.; Keddie, J. L.; Roth, P. J. Reactive Polymorphic Nanoparticles: Preparation via Polymerization-Induced Self-Assembly and Postsynthesis Thiol- Para -Fluoro Core Modification. *Macromol. Rapid Commun.* **2019**, *40*, 1800346.

(20) Lesage de la Haye, J.; Zhang, X.; Chaduc, I.; Brunel, F.; Lansalot, M.; D'Agosto, F. The Effect of Hydrophile Topology in RAFT-Mediated Polymerization-Induced Self-Assembly. *Angew. Chemie Int. Ed.* **2016**, *55*, 3739–3743.

(21) Penfold, N. J. W.; Yeow, J.; Boyer, C.; Armes, S. P. Emerging Trends in Polymerization-Induced Self-Assembly. *ACS Macro Lett.* **2019**, *8*, 1029–1054.

(22) Rieger, J. Guidelines for the Synthesis of Block Copolymer Particles of Various Morphologies by RAFT Dispersion Polymerization. *Macromol. Rapid Commun.* **2015**, *36*, 1458–1471.

(23) Derry, M. J.; Fielding, L. A.; Warren, N. J.; Mable, C. J.; Smith, A. J.; Mykhaylyk, O. O.; Armes, S.

P. In Situ Small-Angle X-Ray Scattering Studies of Sterically-Stabilized Diblock Copolymer Nanoparticles Formed during Polymerization-Induced Self-Assembly in Non-Polar Media. *Chem. Sci.* **2016**, *7*, 5078–5090.

(24) Pei, Y.; Sugita, O. R.; Thurairajah, L.; Lowe, A. B. Synthesis of Poly(Stearyl Methacrylate-b-3-Phenylpropyl Methacrylate) Nanoparticles in n-Octane and Associated Thermoreversible Polymorphism. *RSC Adv.* **2015**, *5*, 17636–17646.

(25) Cunningham, V. J.; Alswieleh, A. M.; Thompson, K. L.; Williams, M.; Leggett, G. J.; Armes, S. P.; Musa, O. M. Poly(Glycerol Monomethacrylate)–Poly(Benzyl Methacrylate) Diblock Copolymer Nanoparticles via RAFT Emulsion Polymerization: Synthesis, Characterization, and Interfacial Activity. *Macromolecules* **2014**, *47*, 5613–5623.

(26) Cockram, A. A.; Neal, T. J.; Derry, M. J.; Mykhaylyk, O. O.; Williams, N. S. J.; Murray, M. W.; Emmett, S. N.; Armes, S. P. Effect of Monomer Solubility on the Evolution of Copolymer Morphology during Polymerization-Induced Self-Assembly in Aqueous Solution. *Macromolecules* **2017**, *50*, 796–802.

(27) Rymaruk, M. J.; Thompson, K. L.; Derry, M. J.; Warren, N. J.; Ratcliffe, L. P. D.; Williams, C. N.; Brown, S. L.; Armes, S. P. Bespoke Contrast-Matched Diblock Copolymer Nanoparticles Enable the Rational Design of Highly Transparent Pickering Double Emulsions. *Nanoscale* **2016**, *8*, 14497–14506.

(28) Zhang, X.; Rieger, J.; Charleux, B. Effect of the Solvent Composition on the Morphology of Nano-Objects Synthesized via RAFT Polymerization of Benzyl Methacrylate in Dispersed Systems. *Polym. Chem.* **2012**, *3*, 1502–1509.

(29) Zaquen, N.; Azizi, W. A. A. W.; Yeow, J.; Kuchel, R. P.; Junkers, T.; Zetterlund, P. B.; Boyer, C. Alcohol-Based PISA in Batch and Flow: Exploring the Role of Photoinitiators. *Polym. Chem.* **2019**, *10*, 2406–2414.

(30) Yeow, J.; Xu, J.; Boyer, C. Polymerization-Induced Self-Assembly Using Visible Light Mediated Photoinduced Electron Transfer-Reversible Addition-Fragmentation Chain Transfer Polymerization. *ACS Macro Lett.* **2015**, *4*, 984–990.

(31) Yeow, J.; Shanmugam, S.; Corrigan, N.; Kuchel, R. P.; Xu, J.; Boyer, C. A Polymerization-Induced Self-Assembly Approach to Nanoparticles Loaded with Singlet Oxygen Generators. *Macromolecules* **2016**, *49*, 7277–7285.

(32) Fielding, L. A.; Derry, M. J.; Ladmiral, V.; Rosselgong, J.; Rodrigues, A. M.; Ratcliffe, L. P. D.; Sugihara, S.; Armes, S. P. RAFT Dispersion Polymerization in Non-Polar Solvents: Facile Production of Block Copolymer Spheres, Worms and Vesicles in n-Alkanes. *Chem. Sci.* **2013**, *4*, 2081–2087.

(33) Fielding, L. A.; Lane, J. A.; Derry, M. J.; Mykhaylyk, O. O.; Armes, S. P. Thermo-Responsive Diblock Copolymer Worm Gels in Non-Polar Solvents. *J. Am. Chem. Soc.* **2014**, *136*, 5790–5798.

(34) Derry, M. J.; Fielding, L. A.; Armes, S. P. Industrially-Relevant Polymerization-Induced Self-Assembly Formulations in Non-Polar Solvents: RAFT Dispersion Polymerization of Benzyl Methacrylate. *Polym. Chem.* **2015**, *6*, 3054–3062.

(35) Rymaruk, M. J.; Hunter, S. J.; O'Brien, C. T.; Brown, S. L.; Williams, C. N.; Armes, S. P. RAFT Dispersion Polymerization in Silicone Oil. *Macromolecules* **2019**, *52*, 2822–2832.

(36) Blanazs, A.; Madsen, J.; Battaglia, G.; Ryan, A. J.; Armes, S. P. Mechanistic Insights for Block Copolymer Morphologies: How Do Worms Form Vesicles? *J. Am. Chem. Soc.* **2011**, *133*,

16581–16587.

(37) Lopez-Oliva, A. P.; Warren, N. J.; Rajkumar, A.; Mykhaylyk, O. O.; Derry, M. J.; Doncom, K. E. B.; Rymaruk, M. J.; Armes, S. P. Polydimethylsiloxane-Based Diblock Copolymer Nano-Objects Prepared in Nonpolar Media via RAFT-Mediated Polymerization-Induced Self-Assembly. *Macromolecules* **2015**, *48*, 3547–3555.

(38) Warren, N. J.; Derry, M. J.; Mykhaylyk, O. O.; Lovett, J. R.; Ratcliffe, L. P. D.; Ladmiral, V.; Blanazs, A.; Fielding, L. A.; Armes, S. P. Critical Dependence of Molecular Weight on Thermoresponsive Behavior of Diblock Copolymer Worm Gels in Aqueous Solution. *Macromolecules* **2018**, *51*, 8357–8371.

(39) Trent, J. S.; Scheinbeim, J. I.; Couchman, P. R. Ruthenium Tetraoxide Staining of Polymers for Electron Microscopy. *Macromolecules* **1983**, *16*, 589–598.

(40) Ilavsky, J.; Jemian, P. R. Irena : Tool Suite for Modeling and Analysis of Small-Angle Scattering. *J. Appl. Crystallogr.* **2009**, *42*, 347–353.

(41) Rizzardo, E.; Chen, M.; Chong, B.; Moad, G.; Skidmore, M.; Thang, S. H. RAFT Polymerization: Adding to the Picture. *Radic. Polym. Kinet. Mech.* **2007**, 104–116.

(42) Zhang, W.; D'Agosto, F.; Dugas, P. Y.; Rieger, J.; Charleux, B. RAFT-Mediated One-Pot Aqueous Emulsion Polymerization of Methyl Methacrylate in Presence of Poly(Methacrylic Acid-Co-Poly(Ethylene Oxide) Methacrylate) Trithiocarbonate Macromolecular Chain Transfer Agent. *Polym. (United Kingdom)* **2013**, *54*, 2011–2019.

(43) Ferji, K.; Venturini, P.; Cleymand, F.; Chassenieux, C.; Six, J. L. In Situ Glyco-Nanostructure Formulation via Photo-Polymerization Induced Self-Assembly. *Polym. Chem.* **2018**, *9*, 2868–2872.

(44) Förster, S.; Zisenis, M.; Wenz, E.; Antonietti, M. Micellization of Strongly Segregated Block Copolymers. *J. Chem. Phys.* **1996**, *104*, 9956–9970.

(45) Oranli, L.; Bahadur, P.; Riess, G. Hydrodynamic Studies on Micellar Solutions of Styrene–Butadiene Block Copolymers in Selective Solvents. *Can. J. Chem.* **1985**, *63*, 2691–2696.

(46) Bluhm, T. L.; Malhotra, S. L. Poly(Styrene-b-Isoprene) Micelles. Effect of Molecular Weight on Micelle Size. *Eur. Polym. J.* **1986**, *22*, 249–251.

(47) Pedersen, J. S. Form Factors of Block Copolymer Micelles with Spherical, Ellipsoidal and Cylindrical Cores. *J. Appl. Crystallogr.* **2000**, *33*, 637–640.

(48) Pei, Y.; Noy, J. M.; Roth, P. J.; Lowe, A. B. Soft Matter Nanoparticles with Reactive Coronal Pentafluorophenyl Methacrylate Residues via Non-Polar RAFT Dispersion Polymerization and Polymerization-Induced Self-Assembly. *J. Polym. Sci. Part A Polym. Chem.* **2015**, *53*, 2326–2335.

(49) Pei, Y.; Thurairajah, L.; Sugita, O. R.; Lowe, A. B. RAFT Dispersion Polymerization in Nonpolar Media: Polymerization of 3-Phenylpropyl Methacrylate in n -Tetradecane with Poly(Stearyl Methacrylate) Homopolymers as Macro Chain Transfer Agents. *Macromolecules* **2015**, *48*, 236–244.

(50) Bang, J.; Jain, S.; Li, Z.; Lodge, T. P.; Pedersen, J. S.; Kesselman, E.; Talmon, Y. Sphere, Cylinder, and Vesicle Nanoaggregates in Poly(Styrene-b-Isoprene) Diblock Copolymer Solutions. *Macromolecules* **2006**, *39*, 1199–1208.

(51) Lovett, J. R.; Derry, M. J.; Yang, P.; Hatton, F. L.; Warren, N. J.; Fowler, P. W.; Armes, S. P. Can Percolation Theory Explain the Gelation Behavior of Diblock Copolymer Worms? *Chem. Sci.*

2018, *9*, 7138–7144.

(52) Verber, R.; Blanazs, A.; Armes, S. P. Rheological Studies of Thermo-Responsive Diblock Copolymer Worm Gels. *Soft Matter* **2012**, *8*, 9915.